The oscillatory electro-oxidation of formic acid: insights on the adsorbates involved from time-resolved ATR-SEIRAS and UV reflectance experiments

Fabian W. Hartl,[1] Hamilton Varela[1] and Angel Cuesta*,[2]

[1]Institute of Chemistry of São Carlos, University of São Paulo, 13560-970 São Carlos SP, Brazil

[2]Department of Chemistry, School of Natural and Computing Sciences, University of Aberdeen, AB24 3UE Aberdeen, Scotland, UK

E-mail: angel.cuestaciscar@abdn.ac.uk

ABSTRACT. Galvanostatic potential oscillations during the oxidation of formic acid were studied by time-resolved Surface-Enhanced Infrared Absorption Spectroscopy in the attenuated total reflection configuration (ATR-SEIRAS) and reflectance measurements in the ultraviolet (UV) region. ATR-SEIRAS allowed monitoring oscillations in the coverage of adsorbed CO (CO_{ad}) and adsorbed bridge-bonded formate ($HCOO_{bi}$), while UV reflectance revealed oscillations in the coverage by specifically adsorbed anions (namely, adsorbed sulfate). The potential oscillations and the coverage of all these species are strongly interconnected, and an analysis of their correlation provides detailed insight into the autocatalytic loop responsible for the emergence of non-linear dynamics.

KEYWORDS: formic acid oxidation, platinum, potential oscillations, pH effect, ATR-SEIRAS, differential reflectance spectroscopy

HIGHLIGHTS

All present species in solution and on the surface compete for active sites

Adsorbed anions and bridge-bonded formate interfere in the removal of adsorbed CO

Formic acid oxidation takes place in a complex, potential dependent network

All active processes have to be considered to understand the catalytic performance

1. Introduction

Formic acid oxidation has attracted much interest for decades, because of its own relevance as a possible fuel in fuel cells [1,2], and because it is seen as a model reaction to understand the oxidation of other small organic molecules, where it often also occurs as an intermediate [3–6]. Formic acid oxidation is known to take place via the dual-pathway mechanism first suggested by Capon and Parsons [7]. One of the two pathways, usually called the indirect path, involves the dehydration of formic acid to adsorbed carbon monoxide (CO_{ad}) [8], whose oxidation to CO_2 requires high overpotentials and, therefore, acts as a poisoning species. The so-called direct path involves, instead, the stepwise dehydrogenation of formic acid to CO_2. In addition to CO_{ad}, only bidentate adsorbed formate ($HCOO_{bi}$) has been detected on the electrode surface during formic acid oxidation, and this species was initially claimed to be the intermediate in the direct path.[9,10] However, current consensus is that, although $HCOO^-$ (and not HCOOH) must be the precursor of the actual reactive intermediate [11–19], $HCOO_{bi}$ is not fulfilling this role. It has been suggested that undetected monodentate adsorbed formate ($HCOO_{mono}$) is the reactive intermediate, and needs to adopt a C-H-down configuration before the last proton-electron transfer to yield CO_2 can proceed [12,16,19]. $HCOO_{bi}$ and $HCOO_{mono}$ are thought to be in equilibrium with each other

[12,19], and, since the rate of formation of CO_{ad} has been shown to increase linearly with the coverage of $HCOO_{bi}$ [13,20], $HCOO_{mono}$ is thought to also be the intermediate in the dehydration of formic acid to CO_{ad} [12,16,19].

Non-linear dynamics phenomena, such as periodic oscillations, quasiperiodicities, and chaos, are common in electrochemical systems [21,22]. The electrocatalytic oxidation of formic acid is one of the most typical and most studied electrochemical oscillators [23–29], known to produce temporal oscillations under both potentiostatic and galvanostatic conditions. Osawa and co-coworkers were the first to use time-resolved surface-enhanced infrared absorption spectroscopy in the attenuated total reflection mode (ATR-SEIRAS) to provide insight into the feedback mechanism responsible for the oscillatory behavior in the electrooxidation of formic acid [28–30]. They found CO_{ad} and $HCOO_{bi}$ to change their coverages synchronously with the temporal potential oscillations [29]. According to their interpretation, CO_{ad} blocks the adsorption of $HCOO_{bi}$, and suppresses the dehydrogenation of $HCOO_{mono}$ to CO_2, provoking an increase in the potential in order to maintain the applied current. When the potential is high enough CO_{ad} is oxidatively removed, allowing for an increase in the coverage of $HCOO_{bi}$ and an acceleration of the dehydrogenation of $HCOO_{mono}$. This results in a negative shift of the potential that leads again to the formation of CO_{ad}, resulting in a self-sustained loop. However, although ATR-SEIRAS is very well suited for the detection of CO_{ad} and $HCOO_{bi}$, it is not so sensitive to the presence of specifically adsorbed anions like adsorbed sulfate. Ultraviolet (UV) reflectance, on the contrary, has been shown to be very sensitive to the presence of a variety of adsorbed species on the surface of Pt electrodes, and, in sulfuric acid solutions, can be used to monitor changes in sulfate coverage [31–39], thus allowing a deeper inside into the feedback mechanism, when the system is oscillating.

Here, we present a study of the species present on the surface of a Pt electrode and the oscillations in their respective coverage during galvanostatic oxidations combining ATR-SEIRAS with UV reflectance measurements. Our ATR-SEIRAS results are completely consistent with previous work by Osawa and co-workers, but we complete their interpretation using new knowledge gathered since that work, particularly about the mechanism of formation of CO_{ad} from HCOOH. Furthermore, UV reflectance provides new important information regarding the synchronous change in the sulfate coverage, and its role in the feedback mechanism.

2. Experimental

All solutions were prepared with K_2SO_4 (BDH Chemicals, 99%), H_2SO_4 (Fisher Scientific, > 95%) and HCOOH (Sigma-Aldrich ≥ 98%). Before each experiment, the electrolyte was deaerated with nitrogen (BOC Gases, 100%).

Galvanostatic potential oscillations were generated using an analogue galvanostat (EG&G Princeton Applied Research (model)), and recorded using a digital oscilloscope (Yokogawa). A reversible hydrogen electrode (RHE) was used as reference, and a Pt wire served as counter electrode.

ATR-SEIRA spectra were carried out using a two-compartment glass cell. The working electrode was a Pt film deposited on the totally reflecting plane of a Si prism bevelled at 60º, following a procedure reported elsewhere.[40] Time-resolved ATR-SEIRAS experiments were performed with a Nicolet 470 FTIR spectrometer equipped with a liquid nitrogen-cooled MCT detector, using unpolarised light. The background spectrum was recorded at 0.10 V in the formic acid-free electrolyte, and consisted of 100 interferograms. Spectra are reported in absorbance units, calculated as $A = -\log\frac{R_{\text{sample}}}{R_{\text{background}}}$, where R_{sample} and $R_{\text{background}}$ are the reflectance of the sample under the sample and background conditions, respectively. Spectral series with an interval of 140

ms between spectra were recorded during galvanostatic potential oscillations, each spectrum in the series consisting of a single interferogram with a spectral resolution of 8 cm^{-1}.

UV reflectance was monitored using a two-compartment Teflon cell especially designed for this purpose. All reflectance experiments were performed at $\lambda = 250$ nm. The working electrode was a Pt(111) single crystal (MaTecK, disk 10 mm in diameter and 2 mm thick) suspended from a Pt wire and completely immersed in the solution (*i.e.*, while the reflectance signal originates exclusively from the oriented face, the electrochemical signal comes from the whole of the disk, and from the fraction of Pt wire immersed in the electrolyte).

3. Results

As demonstrated by Osawa and co-workers [28,29], ATR-SEIRAS can be used to monitor in real time the variations in the coverage of CO_{ad} and $HCOO_{bi}$ associated to galvanostatic oscillations during the electrooxidation of formic acid on Pt. A typical series of spectra acquired simultaneously with a galvanostatic chronopotentiogram showing typical potential oscillations is shown in Figure 1, and are in good agreement with the literature [29]:

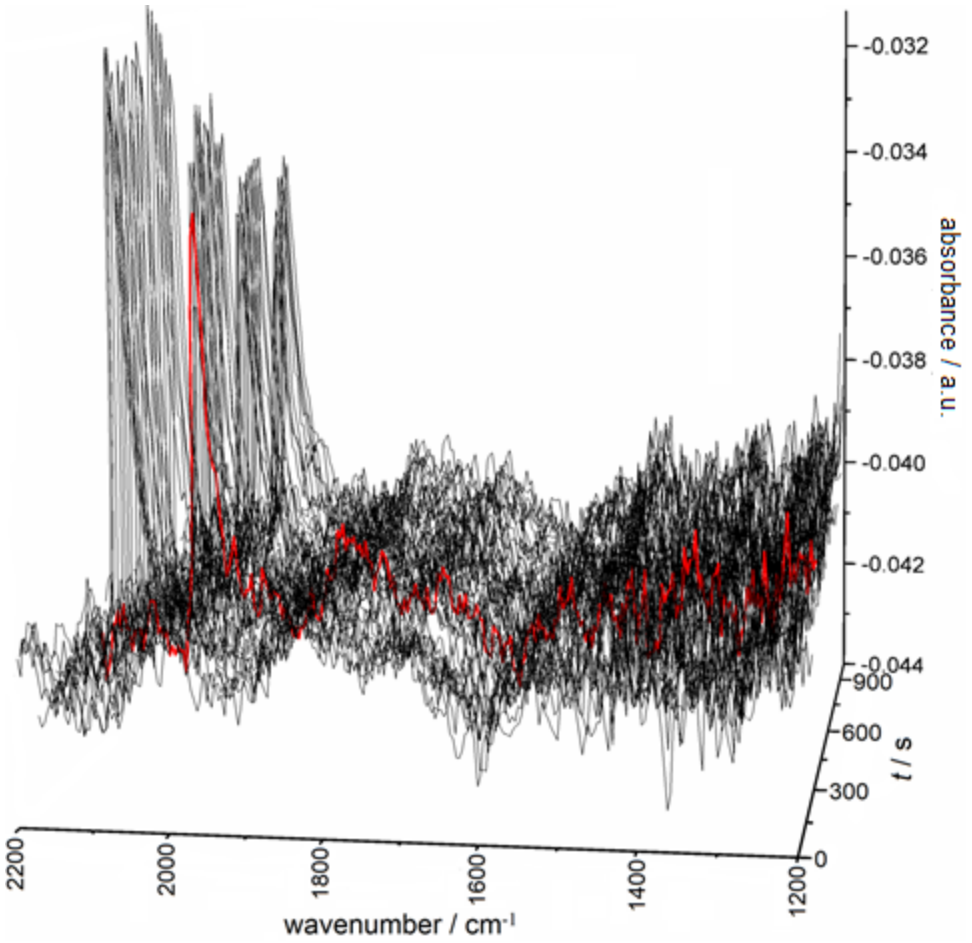

Figure 1. Representative series of ATR-SEIRA spectra recorded simultaneously to the chronopotentiogram of a Pt electrode in 0.3 M K_2SO_4 + 0.1 M H_2SO_4 + 0.4 M HCOOH at 0.15 mA cm^{-2}. The spectrum at 390 s (red line) is representative for the other spectra. Time interval between spectra: 20 s.

Figure 2 shows the time evolution of the electrode potential in 0.3 M K_2SO_4 + 0.1 M H_2SO_4 + 0.4 M HCOOH at a constant current density of 0.15 mA cm^{-2}, alongside the evolution of the stretching frequency of linearly-bonded CO (CO_L) and the integrated intensities of the CO_L and $HCOO_{bi}$ bands (I_{CO} and I_{HCOO}, respectively) in simultaneously recorded ATR-SEIRA spectra. The frequency of the CO_L band, which oscillates in phase with the electrode potential, was used to ensure good synchronization between the electrochemical and spectroscopic parts of the experiments.

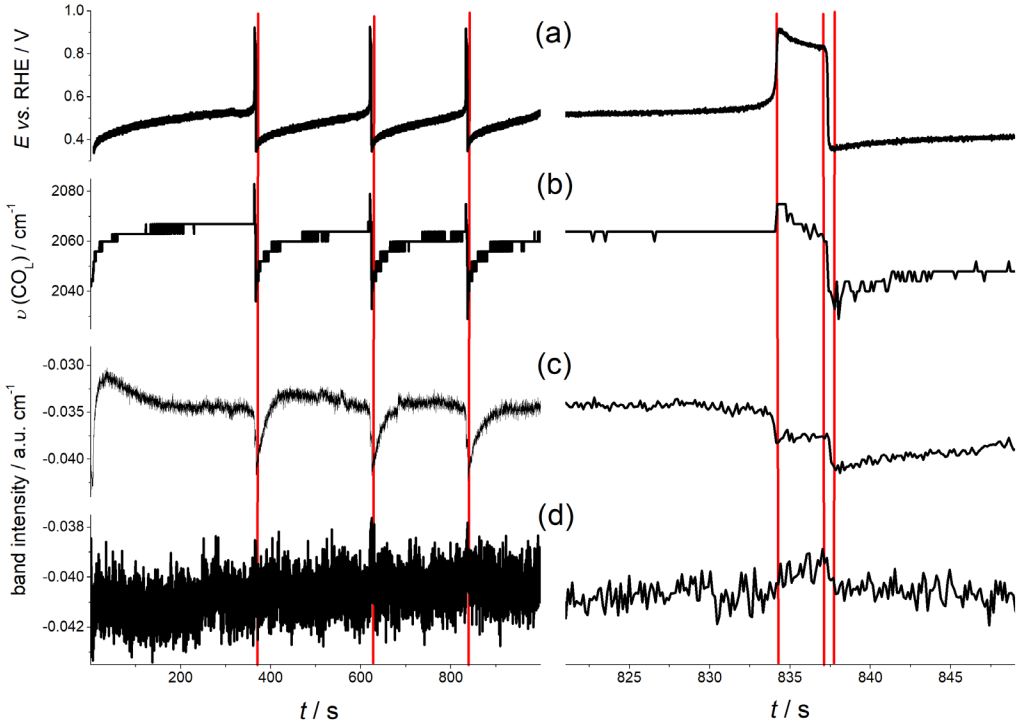

Fig. 2 Potential oscillation pattern for a current density of 0.15 mA cm^{-2} applied to a Pt film deposited on a Si prism (a), stretching frequency of the CO_L band (b), and integrated band intensities of CO_L (c) and $HCOO_{bi}$ (d) obtained from a simultaneously recorded series of ATR-SEIRA spectra. The electrolyte was a 0.3 M K_2SO_4 + 0.1 M H_2SO_4 + 0.4 M HCOOH solution. The panel on the right is an expanded view of the oscillation between 820 and 850 s. The background spectrum was recorded at 0.10 V in the absence of formic acid.

Similar experiments at current densities of 0.27 and 0.35 mA cm^{-2} are shown in the Supporting Information (Figures S1 and S2). Please note that I_{HCOO} can be assumed to be proportional to the coverage of $HCOO_{bi}$ (θ_{HCOO}) [10], while I_{CO} has been shown to be proportional to the CO_{ad} coverage (θ_{CO}) at sufficiently low coverages [41,42]. It is also worth noting that at the positive limit of the potential oscillations (around 0.90 V) barely no CO_{ad} is left on polycrystalline Pt during the oxidation of formic acid [9], and that even a saturated CO adlayer will be oxidized within a fraction of a second at that potential, under potentiostatic or voltammetric conditions [42].

However, under the far-from-equilibrium conditions required for oscillatory behavior to emerge, CO_{ad} is always present on the surface, even at the most positive potential in the oxidation spike (Fig. S3).

Figs. 2, S1 and S2 show that both I_{CO} and I_{HCOO} (and, hence, θ_{CO} and θ_{HCOO}) oscillate synchronously with the potential, in good agreement with previous work [28,29]. Also in agreement with that work, I_{CO} decreases coinciding with the potential spike, while I_{HCOO} increases. Zooming into the oscillation shows that the onset of the potential spike coincides with the onset of the decrease of I_{CO}, which runs sharply until the positive potential limit of the oscillation is reached (see Figs. 2(a) and (c) and Fig. S1). Then, the potential starts decreasing slowly, while I_{CO} stops decreasing (Fig. 2) or also decreases more slowly (Figs. S1 and S2) for a short while, after which a sudden decrease in the potential is accompanied by a sudden decrease in I_{CO} (see also Figs 2, S1, S2 and S3). The lowest potential limit of the oscillation coincides with the lowest I_{CO}, but while initially both the potential and I_{CO} increase in parallel after reaching the lowest potential limit, I_{CO} stops increasing after some seconds, while the potential continues increasing until the new spike appears. This behavior is also reflected in the oscillation of the potential and covergae dependent position of the CO stretching frequency in Fig. 2(b), which perfectly follows the potential profile. This confirms that the decrease in the CO_{ad} coverage must be very small during the short time interval at the higher potentials (otherwise, th einitial increase in the CO stretching frequency due to the increase in potential would be offset by the decrease in frequency due to the decrease in coverage) and then accelerates in the sharp negative potential transient by the end of the oscillation spike.

I_{HCOO} starts increasing coinciding with the positive potential limit of the spike, and keeps on increasing during the slow decrease in potential that follows, except at the highest current density

applied. In this case, I_{HCOO} reaches fast a higher value, which remains constant for the short time period at intermediate potential (Fig. S3). I_{HCOO} starts decreasing coinciding with the sudden decrease of potential at the end of the oscillation spike, and reaches the value before the oscillation coinciding with the lowest potential limit of the oscillation (see Figs. 2, S1 and S2).

Even though not directly involved in the reaction, species present in the electrolyte, particularly specifically adsorbing anions, can interact with the surface, affecting the availability of reaction sites or even the stability of adsorbed reaction intermediates. In sulfuric acid solutions, sulfate adsorption on Pt is known to occur in the potential region within which the potential oscillates in the results shown in Figs. 2, S1, S2 and S3. However, oscillations in the bands corresponding to adsorbed sulfate are difficult to follow using ATR-SEIRAS, as they appear below 1200 cm^{-1} [43], close to the lower limit of the spectral range available with our Si prisms (1150 cm^{-1}), and, furthermore, often interfere with a spurious band of silicon oxide around 1100 cm^{-1}. The oxidation of CO_{ad} also requires the previous formation of an oxygenated species on the Pt surface (usually assumed to be adsorbed OH, OH_{ad}) before CO_2 can be generated in a Langmuir-Hinshelwood step. Formation of oxygenated species can result in an upward shift of the non-resonant background level in ATR-SEIRA spectra, but this typically requires formation of a surface oxide, and ATR-SEIRAS is essentially insensitive to OH_{ad}. Although UV reflectance is sensitive to changes in the coverage of OH_{ad} (θ_{OH}) [36], in sulfuric acid solutions sulfate adsorption dominates the reflectance of a Pt electrode in the potential range of interest [37]. Accordingly, we resorted to UV reflectance spectroscopy to monitor oscillations in the coverage by adsorbed sulfate ($\theta_{sulfate}$) during the galvanostatic oxidation of formic acid in the oscillatory regime.

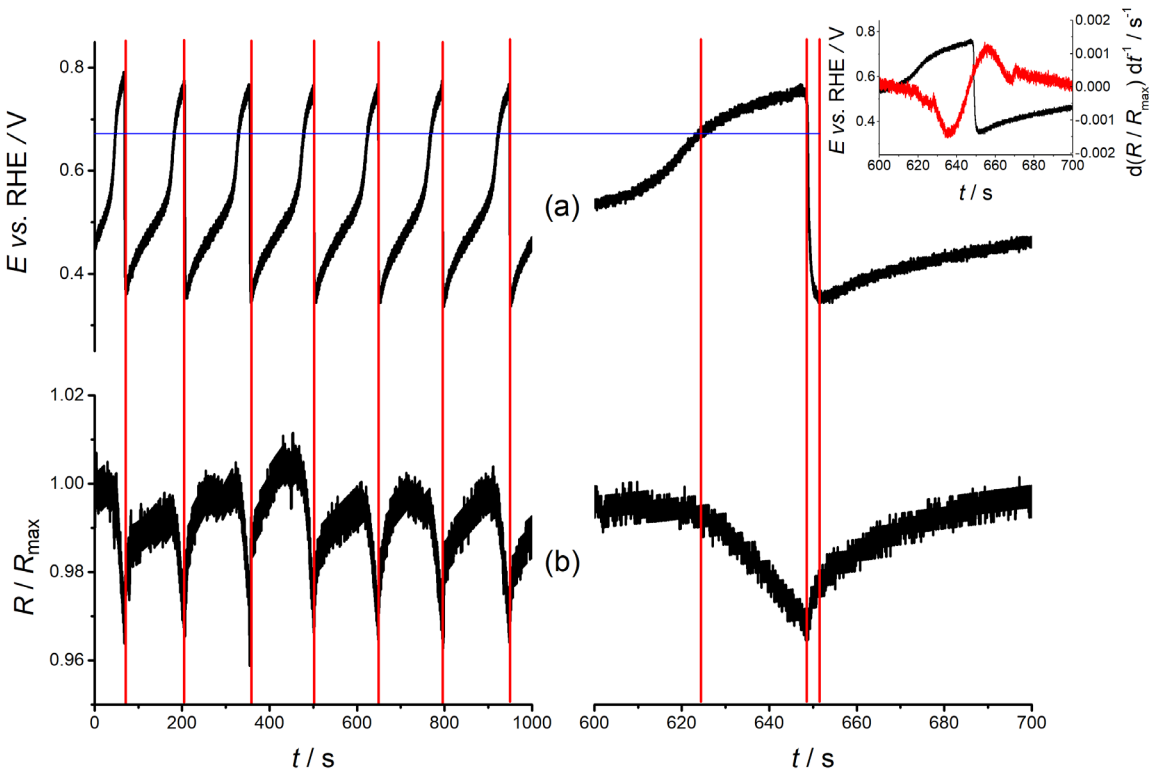

Fig. 3 Potential oscillation pattern for a current of 0.32 mA cm^{-2} applied to a Pt single-crystal disk immersed in 0.3 M K_2SO_4 + 0.1 M H_2SO_4 + 0.4 M HCOOH (a) and the simultaneously recorded relative change in the reflectance of the Pt(111) face at λ = 250 nm (b). The panel on the right is an expanded view of the oscillation between 600 and 700 s. The inset shows a potential oscillation (black) and the derivative of the synchronous reflectance oscillation (red).

Figure 3 shows the time evolution of the potential of a Pt single-crystal disk immersed in 0.3 M K_2SO_4 + 0.1 M H_2SO_4 + 0.4 M HCOOH at a constant current of 0.32 mA cm^{-2}, alongside the relative changes of the reflectance of the Pt(111) face of the single crystal at λ = 250 nm. As in the case of the CO_L and $HCOO_{bi}$ vibrational signatures, the change of the surface reflectance is perfectly synchronized with the potential oscillations. Similar figures at constant currents of 0.67 and 0.80 mA cm^{-2} are shown in the Supporting Information (Figs. S4 and S5). Although sulfate adsorption is favoured on (111) terraces over other surface sites [44] and, therefore, will probably more extensive on Pt(111) than on polycrystalline Pt, preventing a quantitative comparison

between our ATR-SEIRAS and our UV-reflectance studies, a qualitative comparison can still be done, and allows a deeper understanding of the potential-dependent coverage of adsorbates during the oscillating formic acid oxidation.

The difference in the shape of the potential oscillations in Figs. 2 and 3 (and in the corresponding figures in the Supporting Information) is due to the different electrode and setup in the experiment. Despite these differences, the oscillation patterns share the same essential features: a period of slowly rising potential, followed by a faster rise of potential that then levels off, and then a sharp decrease, after which a new cycle starts. The UV reflectance starts decreasing as soon as the potential starts increasing in the potential spike. This is best appreciated in the inset to Figure 3, where the derivative of the reflectance with time has been plotted alongside the potential oscillation. It can be clearly seen that the derivative of the reflectance remains roughly constant and close to zero until the onset of the potential spike. The decrease of the UV reflectance slows down coinciding with the leveling off of the potential increase, and the reflectance reaches a minimum (*i.e.*, θ_{sulfate} reaches a maximum) coinciding with the maximum potential. Then, the reflectance starts increasing again.

Interestingly, the rate at which the reflectance increases grows as the potential decreases, and reaches a maximum between the inflection in the potential transient and the potential maximum, after which the reflectance keeps on decreasing more slowly until the potential maximum and a reflectance minium is reached (see inset in Fig. 3). The difference between the maximum and the minimum reflectance is consistent with previous reports of the decrease of reflectance of a Pt(111) when the potential increases from ca. 0.40 to 0.80 – 0.90 V [37], if the fact that the change in reflectance due to adsorption of sulfate and other species on Pt is larger in the UV region than in the visible is taken into account [38].

4. Discussion

Combining the data provided by Figures 2 and 3 (and the corresponding figures in the Supporting Information) we can obtain a more detailed picture of the connection between the potential oscillations and the oscillations in the coverage of the relevant species, namely, CO_{ad}, adsorbed sulfate and $HCOO_{mono}$ (the latter we will assume to be in equilibrium with $HCOO_{bi}$ [12]), than that previously obtained from only examining ATR-SEIRAS data [29,30]. Initially, during the long period preceding an oscillation, the potential is seen to increase slowly, although no change can be observed in I_{CO}, I_{HCOO} (Fig. 2) and R/R_{max} (Fig. 3). Although this suggests that θ_{CO}, θ_{HCOO} and $\theta_{sulfate}$ remain constant during this part of the chronopotentiogram, this cannot be so, as, otherwise, why would the potential increase at all? We suggest that θ_{CO} is continuously, albeit very slightly, increasing during this part of the oscillation, but this is not reflected in I_{CO} because the coverage is already initially high, above the threshold coverage below which I_{CO} depends linearly on θ_{CO}. Please also note that, although dehydration of formic acid to CO_{ad} does not involve any net electron transfer [13,20], it follows an electrochemical mechanism, and the rate of formation of CO_{ad} will decrease as the potential increases.

As θ_{CO} increases, formic acid oxidation becomes more and more difficult, and the potential needs to increase significantly in order to sustain the current demanded by the galvanostat. Eventually, the potential will need to shoot up to allow for OH_{ad} nucleation on the surface, originating the positive potential spike and igniting the oxidation of CO_{ad}. Interestingly, the sudden rise in potential coincides with a sudden decrease (Fig. 2) in I_{CO} (and, therefore, θ_{CO}) and a not so sharp decrease of R/R_{max} (Fig. 3), while I_{HCOO} remains roughly constant (Fig. 2). This suggests that the places left free by CO_{ad} are occupied mainly by adsorbed sulfate rather than $HCOO_{bi}$. The slower decrease of R/R_{max} as compared with I_{CO} is at odds with the observation of a comparable

decrease and increase in θ_{CO}, and $\theta_{sulfate}$, respectively during the oxidation of CO in CO-saturated solutions under similar conditions [37]. Although OH_{ad}, also needs to form on the electrode surface for the oxidation of CO_{ad} to proceed, and although the projected area of sulfate on the electrode surface is larger than that of CO_{ad}, and therefore more than one CO must be removed from the surface to allow for the adsorption of one sulfate, this cannot explain the differences between this work and ref. [37]. However, while only adsorbed CO, sulfate and adsorbed oxygenated species can compete for adsorption sites in ref. [37], here formate (both $HCOO_{bi}$ detected by IR and the more weakly adsorbed reactive intermediate, which must certainly be present on the surface, as the reaction is continuously sustained during the galvanostatic experiment) is also competing for any adsorption site left free, which will necessarily affect the rate at which the sulphate coverage increases.

Immediately after the sudden positive potential spike and the concomitant sudden decrease of I_{CO}, the change of both magnitudes slows down, while I_{HCOO} starts increasing (Fig. 2) and the decrease of R/R_{max} accelerates (Fig. 3). This suggests that after the initial sharp decrease in θ_{CO}, adsorbed sulfate and $HCOO_{bi}$ outcompete OH_{ad} for the adsorption sites left free by CO_{ad}. The decrease in θ_{CO} also results in a decrease of the rate at which CO_{ad} is oxidized, as this reaction follows a Langmuir-Hinshelwood mechanism the rate of which will be given by the product between θ_{CO} and θ_{OH}. Both θ_{HCOO} and $\theta_{sulfate}$ reach a maximum coinciding with the maximum in potential.

Eventually, θ_{CO} will be low enough for the mobility of CO_{ad} on the surface to increase considerably and diffuse faster to those sites where OH_{ad} is available [45–47], generating a sharp decrease in θ_{CO} and in the potential (Fig. 1), as the catalytic poison is removed and the reaction can proceed again through the direct path at a sufficient rate to maintain the demanded current. It

is worth noting that the sharp decrease in potential coincides with a decrease in I_{HCOO} and an increase in R/R_{max} (*i.e.*, a decrease in both θ_{HCOO} and $\theta_{sulfate}$). This is to be expected, as both species are specifically adsorbed anions, whose adsorption is favored at more positive potentials. θ_{HCOO} does not change further after the potential minimum (Fig. 2), while R/R_{max} continues increasing (Fig. 3). The latter suggests the gradual displacement of adsorbed sulfate by CO_{ad}, which has been shown to generate from adsorbed formate and to require a minimum atomic ensemble of three contiguous atoms [13,20,48]. Simulations of the galvanostatic oscillations during formic acid oxidation on Pt based on a model considering only CO_{ad} and $HCOO_{bi}$ have been shown to reproduce most of the experimental features [28]. Our results clearly indicate that the model could be further improved if a more complex network including other surface processes like anion adsorption is considered, thereby leading to a deeper understanding of non-linear reaction dynamics.

5. Conclusions

In summary, our results show that potential oscillations during the galvanostatic electro-oxidation of formic acid are the result of a complex autocatalytic loop, involving not only the reactive intermediate ($HCOO_{mono}$) and the catalytic poison (CO_{ad}), but also OH_{ad} (necessary to remove CO_{ad}) and spectator species (adsorbed sulfate in this case), as well as species connected to the reaction mechanism but not directly involved in it (namely, $HCOO_{bi}$).

ASSOCIATED CONTENT

Supporting Information: Figures S1 to S5.

ACKNOWLEDGMENT

The support of the University of Aberdeen is gratefully acknowledged. F.W.H. and H.V. acknowledge São Paulo Research Foundation (FAPESP) for the scholarship (grant #2014/08030-9, grant #2017/07286-8) and financial support (grant #2013/16930-7). HV (grant #306151/2010-3) acknowledges Conselho Nacional de Desenvolvimento Científico e Tecnológico (CNPq) for financial support. This study was also supported by the Coordenação de Aperfeiçoamento de Pessoal de Nível Superior - Brasil (CAPES) - Finance Code 001.

REFERENCES

[1] C. Rice, S. Ha, R.I. Masel, A. Wieckowski, Catalysts for direct formic acid fuel cells, J. Power Sources. 115 (2003) 229–235. doi:10.1016/S0378-7753(03)00026-0.

[2] C. Rice, S. Ha, R.I. Masel, P. Waszczuk, A. Wieckowski, T. Barnard, Direct formic acid fuel cells, J. Power Sources. 111 (2002) 83–89. doi:10.1016/S0378-7753(02)00271-9.

[3] E.A. Batista, G.R.P. Malpass, A.J. Motheo, T. Iwasita, New insight into the pathways of methanol oxidation, Electrochem. Commun. 5 (2003) 843–846. doi:10.1016/j.elecom.2003.08.010.

[4] E.A. Batista, G.R.P. Malpass, A.J. Motheo, T. Iwasita, New mechanistic aspects of methanol oxidation, J. Electroanal. Chem. 571 (2004) 273–282. doi:10.1016/j.jelechem.2004.05.016.

[5] E.A. Batista, T. Iwasita, Adsorbed Intermediates of Formaldehyde Oxidation and Their Role in the Reaction Mechanism, Langmuir. 22 (2006) 7912–7916. doi:10.1021/la061182z.

[6] H. Wang, T. Löffler, H. Baltruschat, Formation of intermediates during methanol oxidation: A quantitative DEMS study, J. Appl. Electrochem. 31 (2001) 759–765. doi:10.1023/A:1017539411059.

[7] A. Capon, R. Parsons, The oxidation of formic acid at noble metal electrodes Part III. Intermediates and mechanism on platinum electrodes, J. Electroanal. Chem. Interfacial Electrochem. 45 (1973) 205–231. doi:https://doi.org/10.1016/S0022-0728(73)80158-5.

[8] B. Beden, A. Bewick, C. Lamy, A study by electrochemically modulated infrared reflectance spectroscopy of the electrosorption of formic acid at a platinum electrode, J. Electroanal. Chem. Interfacial Electrochem. 148 (1983) 147–160. doi:https://doi.org/10.1016/S0022-0728(83)80137-5.

[9] Y.X. Chen, A. Miki, S. Ye, H. Sakai, M. Osawa, Formate, an Active Intermediate for Direct Oxidation of Methanol on Pt Electrode, J. Am. Chem. Soc. 125 (2003) 3680–3681. doi:10.1021/ja029044t.

[10] M. Osawa, K. Komatsu, G. Samjeské, T. Uchida, T. Ikeshoji, A. Cuesta, C. Gutiérrez, The Role of Bridge-Bonded Adsorbed Formate in the Electrocatalytic Oxidation of Formic Acid on Platinum, Angew. Chemie Int. Ed. 50 (2011) 1159–1163. doi:10.1002/anie.201004782.

[11] S. Brimaud, J. Solla-Gullón, I. Weber, J.M. Feliu, R.J. Behm, Formic Acid Electrooxidation on Noble-Metal Electrodes: Role and Mechanistic Implications of pH, Surface Structure, and Anion Adsorption, ChemElectroChem. 1 (2014) 1075–1083. doi:10.1002/celc.201400011.

[12] A. Cuesta, Formic acid oxidation on metal electrodes, in: K. Wandelt (Ed.), Encycl. Interfacial Chem. Surf. Sci. Electrochem. Vol. 5, Elsevier, 2018: pp. 620–632.

[13] A. Cuesta, G. Cabello, M. Osawa, C. Gutiérrez, Mechanism of the Electrocatalytic Oxidation of Formic Acid on Metals, ACS Catal. 2 (2012) 728–738. doi:10.1021/cs200661z.

[14] J. Joo, T. Uchida, A. Cuesta, M.T.M. Koper, M. Osawa, The effect of pH on the electrocatalytic oxidation of formic acid/formate on platinum: A mechanistic study by surface-enhanced infrared spectroscopy coupled with cyclic voltammetry, Electrochim. Acta. 129 (2014) 127–136. doi:10.1016/j.electacta.2014.02.040.

[15] J. Joo, T. Uchida, A. Cuesta, M.T.M. Koper, M. Osawa, Importance of Acid–Base Equilibrium in Electrocatalytic Oxidation of Formic Acid on Platinum, J. Am. Chem. Soc. 135 (2013) 9991–9994. doi:10.1021/ja403578s.

[16] A. Ferre-Vilaplana, J. V Perales-Rondón, C. Buso-Rogero, J.M. Feliu, E. Herrero, Formic

acid oxidation on platinum electrodes: A detailed mechanism supported by experiments and calculations on well-defined surfaces, J. Mater. Chem. A. (2017). doi:10.1039/C7TA07116G.

[17] F.W. Hartl, H. Varela, The Effect of Solution pH and Temperature on the Oscillatory Electro-Oxidation of Formic Acid on Platinum, ChemistrySelect. 2 (2017) 8679–8685. doi:10.1002/slct.201702008.

[18] J. V Perales-Rondón, S. Brimaud, J. Solla-Gullón, E. Herrero, R. Jürgen Behm, J.M. Feliu, Further Insights into the Formic Acid Oxidation Mechanism on Platinum: pH and Anion Adsorption Effects, Electrochim. Acta. 180 (2015) 479–485. doi:http://dx.doi.org/10.1016/j.electacta.2015.08.155.

[19] E. Herrero, J.M. Feliu, Understanding formic acid oxidation mechanism on platinum single crystal electrodes, Curr. Opin. Electrochem. (2018). doi:10.1016/J.COELEC.2018.03.010.

[20] A. Cuesta, G. Cabello, C. Gutierrez, M. Osawa, Adsorbed formate: the key intermediate in the oxidation of formic acid on platinum electrodes, Phys. Chem. Chem. Phys. 13 (2011) 20091–20095.

[21] M.T.M. Koper, Oscillations and Complex Dynamical Bifurcations in Electrochemical Systems, in: I. Prigogine, S.A. Rice (Eds.), Adv. Chem. Physics, Vol 92, Wiley-Blackwell, 2007: pp. 161–298. doi:10.1002/9780470141519.ch2.

[22] K. Krischer, Principles of Temporal and Spatial Pattern Formation in Electrochemical Systems, in: B.E. Conway, J.O. Bockris, R.E. White (Eds.), Mod. Asp. Electrochem. Vol 32, Kluwer Academic Publishers, Boston, 2002: pp. 1–142. doi:10.1007/0-306-46916-2_1.

[23] E. Müller, Zur elektrolytischen Oxydation der Ameisensäure, Zeitschrift Für Elektrochemie Und Angew. Phys. Chemie. 33 (1927) 561–568. doi:10.1002/bbpc.19270331210.

[24] E. Müller, S. Tanaka, Über die pulsierende elektrolytische Oxydation der Ameisensäure, Zeitschrift Für Elektrochemie Und Angew. Phys. Chemie. 34 (1928) 256–264. doi:10.1002/bbpc.19280340510.

[25] P. Strasser, M. Eiswirth, G. Ertl, Oscillatory instabilities during formic acid oxidation on Pt(100), Pt(110) and Pt(111) under potentiostatic control. II. Model calculations, J. Chem. Phys. 107 (1997) 991–1003. doi:10.1063/1.474451.

[26] H. Okamoto, N. Tanaka, M. Naito, Modelling temporal kinetic oscillations for electrochemical oxidation of formic acid on Pt, Chem. Phys. Lett. 248 (1996) 289–295. doi:10.1016/0009-2614(95)01295-8.

[27] F.N. Albahadily, M. Schell, Observation of several different temporal patterns in the oxidation of formic acid at a rotating platinum-disk electrode in an acidic medium, J. Electroanal. Chem. Interfacial Electrochem. 308 (1991) 151–173. doi:10.1016/0022-0728(91)85064-V.

[28] Y. Mukouyama, M. Kikuchi, G. Samjeské, M. Osawa, H. Okamoto, Potential Oscillations in Galvanostatic Electrooxidation of Formic Acid on Platinum: A Mathematical Modeling and Simulation, J. Phys. Chem. B. 110 (2006) 11912–11917. doi:10.1021/jp061129j.

[29] G. Samjeské, A. Miki, S. Ye, A. Yamakata, Y. Mukouyama, H. Okamoto, M. Osawa, Potential Oscillations in Galvanostatic Electrooxidation of Formic Acid on Platinum: A Time-Resolved Surface-Enhanced Infrared Study, J. Phys. Chem. B. 109 (2005) 23509–23516. doi:10.1021/jp055220j.

[30] G. Samjeské, M. Osawa, Current Oscillations during Formic Acid Oxidation on a Pt Electrode: Insight into the Mechanism by Time-Resolved IR Spectroscopy, Angew. Chemie Int. Ed. 44 (2005) 5694–5698. doi:10.1002/anie.200501009.

[31] M.A. Barret, R. Parsons, Reflectance studies of absorption on a platinum electrode, Symp. Faraday Soc. 4 (1970) 72–84.

[32] A. Cuesta, C. Gutiérrez, Confirmation by differential reflectance spectroscopy of the transition at 270 nm of CO chemisorbed on Pt in an acid medium, J. Electroanal. Chem. 383 (1995) 195–197. doi:https://doi.org/10.1016/0022-0728(94)03760-Z.

[33] I. Fromondi, A.L. Cudero, J. Feliu, D.A. Scherson, In Situ UV-Visible Reflectance Spectroscopy on Single Crystal Pt(111) Microfacets, Electrochem. Solid-State Lett. 8 (2005) E9–E11. doi:10.1149/1.1830396.

[34] I. Fromondi, D. Scherson, (Bi)Sulfate Adsorption on Quasiperfect Pt(111) Facets from Acidic Aqueous Electrolytes as Monitored by Optical Techniques, J. Phys. Chem. C. 111 (2007) 10154–10157. doi:10.1021/jp073330f.

[35] I. Fromondi, D. Scherson, Surface dynamics at well-defined single crystal microfacetted Pt(111) electrodes: in situ optical studies, Faraday Discuss. 140 (2009) 59–68.

[36] I. Fromondi, D.A. Scherson, Oxidation of Adsorbed CO on Pt(111) in CO-Saturated Perchloric Acid Aqueous Solutions: Simultaneous In Situ Time-Resolved Reflectance Spectroscopy and Second Harmonic Generation Studies, J. Phys. Chem. B. 110 (2006) 20749–20751. doi:10.1021/jp0653095.

[37] I. Fromondi, H. Zhu, D.A. Scherson, In Situ Spectroscopy at the Quasi-Perfect Pt(111) Single-Crystal Facet|Aqueous Electrolyte Interface, J. Phys. Chem. C. 116 (2012) 19613–19624. doi:10.1021/jp3024414.

[38] M. Hachkar, M.C. de Martinez, A. Rakotondrainibe, B. Beden, C. Lamy, Oscillating electrocatalytic systems: Part II. “In situ” UV-visible reflectance spectroscopic investigation of formaldehyde oxidation on rhodium in alkaline medium, J. Electroanal.

Chem. Interfacial Electrochem. 302 (1991) 173–189. doi:https://doi.org/10.1016/0022-0728(91)85039-R.

[39] P. Shi, I. Fromondi, D.A. Scherson, In Situ, Time-Resolved Reflectance Spectroscopy in the Microsecond Domain: Oxidation of Adsorbed Carbon Monoxide on Polycrystalline Pt Microelectrodes in Aqueous Solutions, Langmuir. 22 (2006) 10389–10398. doi:10.1021/la061497e.

[40] A. Miki, S. Ye, M. Osawa, Surface-enhanced IR absorption on platinum nanoparticles: an application to real-time monitoring of electrocatalytic reactions, Chem. Commun. (2002) 1500–1501.

[41] M. Heinen, Y.X. Chen, Z. Jusys, R.J. Behm, In situ ATR-FTIRS coupled with on-line DEMS under controlled mass transport conditions—A novel tool for electrocatalytic reaction studies, Electrochim. Acta. 52 (2007) 5634–5643. doi:https://doi.org/10.1016/j.electacta.2007.01.055.

[42] G. Samjeské, K. Komatsu, M. Osawa, Dynamics of CO Oxidation on a Polycrystalline Platinum Electrode: A Time-Resolved Infrared Study, J. Phys. Chem. C. 113 (2009) 10222–10228. doi:10.1021/jp900582c.

[43] K. Ataka, M. Osawa, In Situ Infrared Study of Water−Sulfate Coadsorption on Gold(111) in Sulfuric Acid Solutions, Langmuir. 14 (1998) 951–959. doi:10.1021/la971110v.

[44] K. Kunimatsu, M.G. Samant, H. Seki, In-situ FT-IR spectroscopic study of bisulfate and sulfate adsorption on platinum electrodes: Part 1. Sulfuric acid, J. Electroanal. Chem. Interfacial Electrochem. 258 (1989) 163–177. doi:https://doi.org/10.1016/0022-0728(89)85170-8.

[45] A. López-Cudero, A. Cuesta, C. Gutiérrez, Potential dependence of the saturation CO

coverage of Pt electrodes: The origin of the pre-peak in CO-stripping voltammograms. Part 1: Pt(111), J. Electroanal. Chem. 579 (2005) 1–12. doi:http://dx.doi.org/10.1016/j.jelechem.2005.01.018.

[46] A. Cuesta, A. Couto, A. Rincón, M.C. Pérez, A. López-Cudero, C. Gutiérrez, Potential dependence of the saturation CO coverage of Pt electrodes: The origin of the pre-peak in CO-stripping voltammograms. Part 3: Pt(poly), J. Electroanal. Chem. 586 (2006) 184–195. doi:10.1016/j.jelechem.2005.10.006.

[47] A. López-Cudero, Á. Cuesta, C. Gutiérrez, Potential dependence of the saturation CO coverage of Pt electrodes: The origin of the pre-peak in CO-stripping voltammograms. Part 2: Pt(100), J. Electroanal. Chem. 586 (2006) 204–216. doi:http://dx.doi.org/10.1016/j.jelechem.2005.10.003.

[48] A. Cuesta, M. Escudero, B. Lanova, H. Baltruschat, Cyclic Voltammetry, FTIRS, and DEMS Study of the Electrooxidation of Carbon Monoxide, Formic Acid, and Methanol on Cyanide-Modified Pt(111) Electrodes, Langmuir. 25 (2009) 6500–6507. doi:10.1021/la8041154.

Graphical abstract: